ISSN: 2639-7536

Research Article

Petroleum and Chemical Industry International

Plasmonic Refractive Index Sensor Including Two Waveguides, Rings and Two Cavities with Teeth Connected on Fano Resonances

Hamid Abbasi*

University of Mazandaran, Iran

***Corresponding Author**
Hamid Abbasi, University of Mazandaran, Iran.

Submitted: 2023, July 15; **Accepted**: 2023, Aug 10: **Published**: 2023, Aug 16

Citation: Abbasi, H. (2023). Plasmonic Refractive Index Sensor Including Two Waveguides, Rings and Two Cavities with Teeth Connected on Fano Resonances. *Petro Chem Indus Intern, 6*(4), 240-247.

Abstract

A plasmonic refractive index sensor based on a metal-insulator-metal (MIM) waveguide coupled with rings and two cavities and interconnected teeth is proposed and investigated numerically. Transfer (T), sensitivity (S) and Figure of Merit (FOM) were calculated and analysed via Finite Difference Time Domain method (FDTD). The simulation results show the generation of double Fano resonances in the system that the resonance line-shapes and the resonance wavelength can be adjusted by changing the geometry of the device. By optimizing the structure in the initial configuration, the maximum sensitivity of 2832 nm / RIU and FOM of 15.1 is achieved. Then we change the structure parameters and the number of resonators. In this case, the maximum sensitivity and FOM are 2083nm / RIU and 18.9 respectively. Therefore two detection points can be used for the refractive index sensor. Such a plasmonic sensor with simple and optimal framework could be suitable and practical for sensing systems and integrated optical circuits.

Keywords: Refractive Index Sensor, Surface Plasmon-Polaritons, Mime Waveguide, Optics, Plasmonic.

1. Introduction

Surface plasmon polaritons (SPPs) are electromagnetic fields propagating along the interface of metal-insulator, and have been debated for decades due to the ability to modulate light in nanoscale as well as break the diffraction limit [1,2]. Plasmon surface polaritons can also be used to transfer data in high-density photonic integrated circuits [3]. The importance of plasmon surface polaritons has led to the study and design of various types of plasmonic devices such as filters, absorbers, splitters and sensors, among which plasmonic sensors have attracted more attention because they are much smaller in size comparable to sensor performance. This means that they are more suitable for integrating [4-10]. So far, various sensors such as refractive index sensors, temperature sensors, phase sensors and gas sensors have been designed and analyse. A sensor must have high sensitivity (S) and high competence (FOM) to have excellent performance and quality. Therefore, these two factors must be evaluated [11-15]. Fano resonance is used to improve the performance of sensitivity and figure of merit (FOM) which results from structure symmetry break or dark-bright resonance interference, and it has an asymmetric spectral line shape with narrow FWHM that is very sensitive to changes in structure parameters and surrounding environment [16-22]. This phenomenon occurs when a discrete state is paired with a continuous state and can also be caused by the interaction between a wide bright mode and a narrow dark mode [23,24]. Also in this research, metal-insulation-metal waveguide (MIM) is used to create a regular and quality structure. Because this waveguide has many features such as high wavelength propagation amplitude, overcoming the diffraction limit and the capability to confine light within considerable propagating length [25-32]. These structures will also increase the speed of information processing by integrating integrated electronic and photonic features [33]. In this paper, we propose a refractive index sensor with a simple plasmonic structure consisting of two waveguides, rings and two cavities with interconnected teeth. The transmission spectrum, and magnetic field distributions | Hz | are simulated by the Two-dimensional time domain (FDTD) with completely matched layer boundary conditions (PML) and simulation parameters, Δ x and Δy equal to 8 nm, are simulated. The results indicate the design of a sensor with proper and regular operation.

2. Theory Analysis and Structural Model

As shown in Fig.1, the proposed structure has two waveguides, a ring and two cavities. Each cavity has ten teeth. The width of the two waveguides is equal to W = 50 nm. The middle ring, which is located in the middle of two waveguides, has an inner radius of r = 152 nm and an outer radius of R = 192 nm. The cavities have a length of L = 565 nm and a height of H1 = H2 = 25 nm. The teeth have a length of g = 25 nm and a height of h = 85 nm. According to the results obtained from several simulations, the best performance of the proposed sensor is obtained when the distance between the cavities and the waveguide is D = 287.5 nm and the distance between the teeth and the waveguide is d = 220 nm.

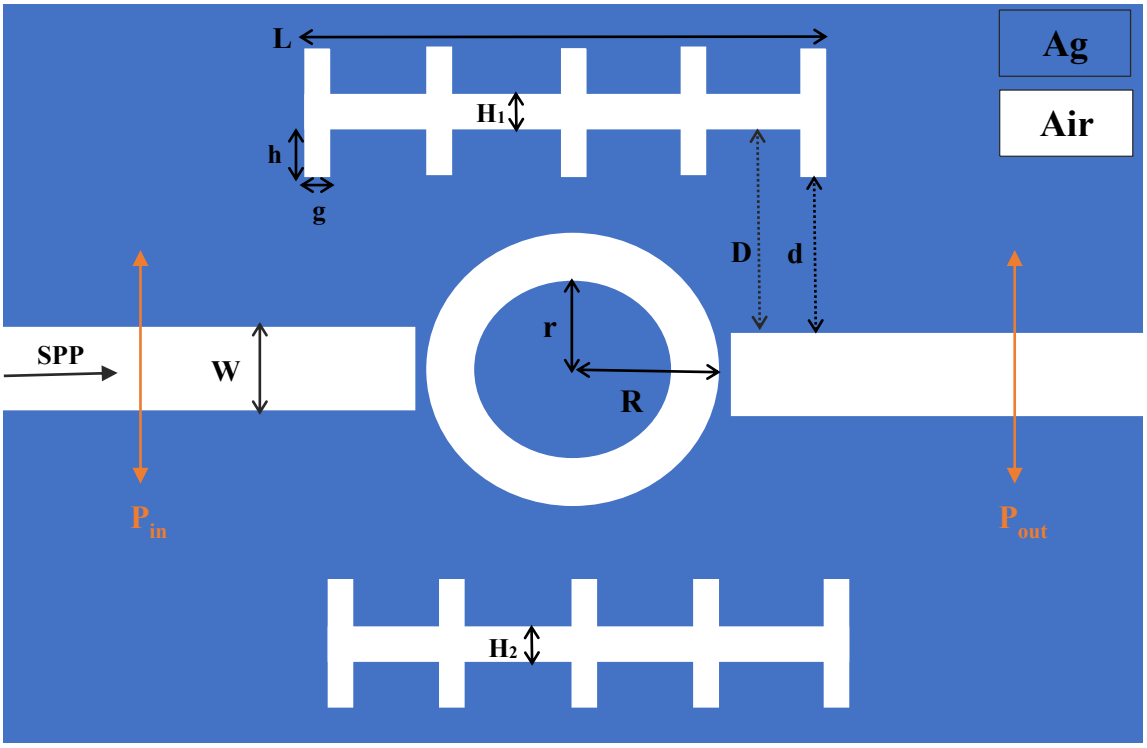

Figure 1: 2D picture of the proposed plasmonic sensor.

The simulation substrate is made of silver to reduce the relative losses in the sensor [34]. As shown in 2D picture (fig.1), the Blue and white areas represent silver and air, respectively. The permittivity of air is set as ε_i=1, as for silver (Ag) the Drude model is utilized as follows [4,35]:

$$\varepsilon(\omega) = \varepsilon_\infty - \frac{{\omega_p}^2}{\omega^2 + i\gamma\omega} \qquad (1)$$

Here ε_∞ =1 gives the medium constant for the infinite frequency, ω_p = 1.37 × 1016 refers to bulk frequency for plasma, γ = 3.21 × 1013 means damping frequency for electron oscillation, and ω shows incident light angular frequency. The Droud model provides a microscopic description of metal dynamics in the form of classical sentences. According to Fig.1, the electromagnetic spectrum enters the device from the left and exits from the right, and to collect the incident and transmitted power, two monitors are put respectively at P_{in} and P_{out}. The transmittance (T) can be calculated by the following equation:

$$T = P_{out} / P_{in} \qquad (2)$$

Surface plasmon polaritons can propagate at the surface of the interface in the waveguide when coupled into the MIM structure. Given that the incident wavelength the width of the bus waveguide is much smaller, and given the scattering relationship of the Surface plasmon polariton, we conclude that only the TM base state exists in the Surface plasmon polariton. The dispersion relation of this fundamental mode is described as follows [25]:

$$\frac{\varepsilon_i\, p}{\varepsilon_m k} = \frac{1 - e^{kw}}{1 + e^{kw}} \qquad (3)$$

$$k = k_0 \sqrt{(\frac{\beta_{sp}}{k_0})^2 - \varepsilon_i} \qquad (4)$$

$$p = k_0 \sqrt{(\frac{\beta_{sp}}{k_0})^2 - \varepsilon_m} \qquad (5)$$

$$\beta_{sp} = n_{eff} k_0 = n_{eff} \frac{2\pi}{\lambda} \qquad (6)$$

Here k0=2π/λ means wave number, ω refer to the width of bus waveguide, εi and εm give the relative dielectric and metal permittivity, λ shows incident light wavelength in vacuum, and βspp and neff are propagation constant and effective refractive index of Surface plasmon polaritons (SPPs). The optical responses of the structure and distribution of the |Hz| simulated and calculated by Finite Difference Time Domain (FDTD) method with the PML boundary conditions. The purpose of using PML is to absorb waves inside the structure and prevent the impact of unwanted reflection waves in the simulation environment. We will calculate the resonant wavelength in terms of effective refractive index using the standing wave theory [36]:

$$\lambda_m = \frac{2Re(n_{eff})}{m - \varphi/\pi} \qquad (7)$$

Re (neff) is the real part of the refractive index, and the phase shift Φ is due to the reflection of light from the metal-air interface in the resonant cavity. L is the effective length of the resonant cavities, and m is the order of resonant mode, which is an integer. The addition of teeth and cavities in the sensor structure changes the amplitude and phase of the propagated wave and changes the shape of the transmission spectrum line, causing resonance peaks in the transmission line, and when the structure is entirely simulated, it has four fano resonance at λ= 465.7 nm, λ= 587.4 nm, λ=858.1 nm, and λ=1677.3 nm (Fig.2).

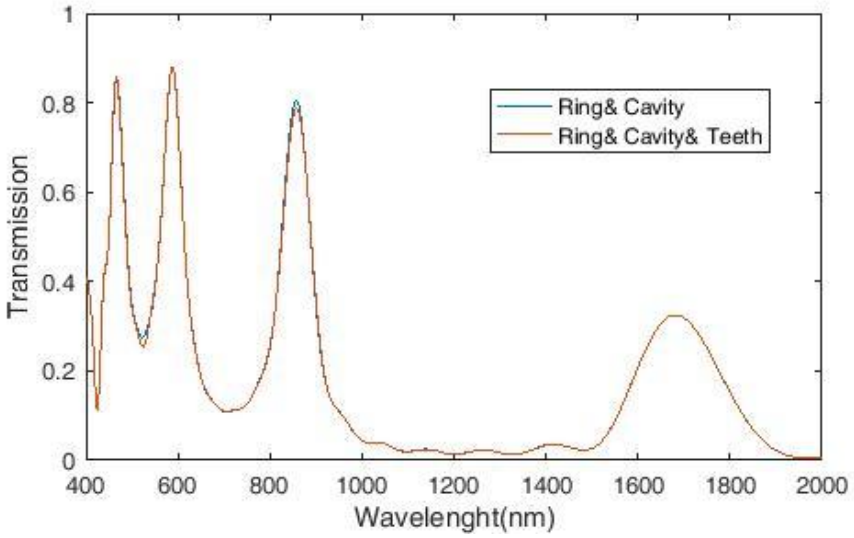

Figure 2: Plasmonic transmission spectrum with rings, cavities and teeth.

To better understand the mechanism of the transmission spectrum, the field distribution | Hz | in resonance peaks and dips studied. As shown in Fig.3, SPPs are inserted through the pin port and then propagated in the waveguide, and when the wavelength reaches to resonance point, most of them are coupled to the ring. As shown in the figure, field distribution |Hz|, showing that in which part of the sensor structure the electromagnetic field is concentrated. We conclude that the maximum radiation is in the middle ring and the Fano resonance is the result of the interaction between the narrow resonance caused by the middle ring and the wide resonance caused by the MIM.

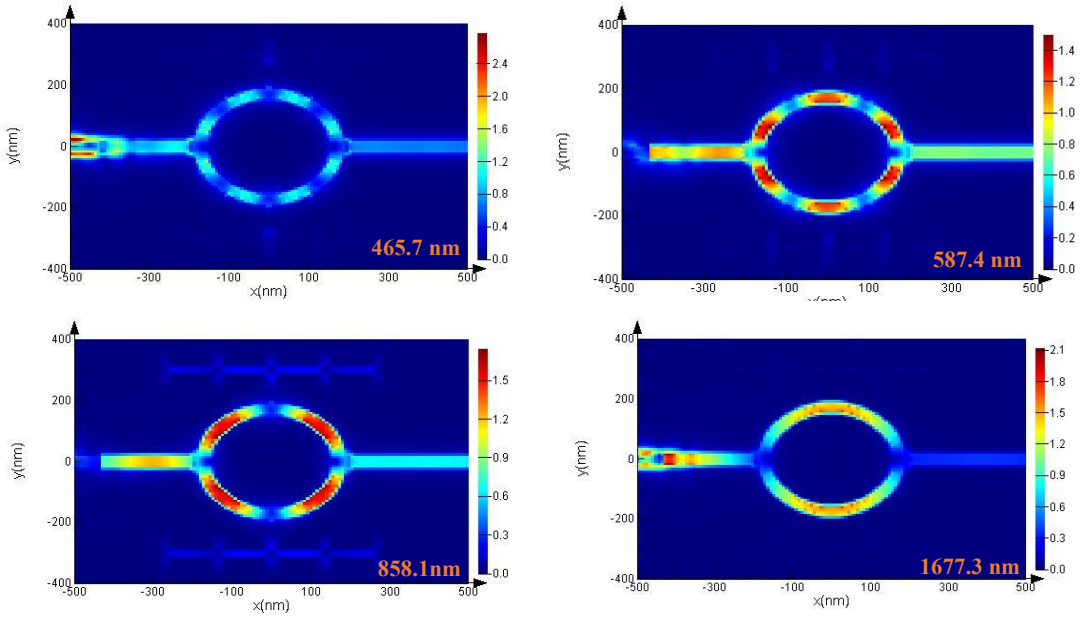

Figure 3: Display of field distribution |Hz| in structure at the resonance wavelengths λ= 465.7 nm, λ= 587.4 nm, λ=858.1 nm, and λ=1677.3 nm.

3. Simulation Methods and Plasmonic Refractive Index Sensor

After designing the structure of the plasmonic sensor, its simulation begins using the Finite Difference Time Domain (FDTD) method. To reduce the simulation time and achieve the desired result, two-dimensional simulation is performed. The uniform mesh size (simulation parameters) for the x and y directions is 8 nm. Two important factors for examining the characteristics of a plasmonic structure are sensitivity (S) and Figure of Merit (FOM). By changing the structure Refractive index, the calculation of sensitivity (S) and Figure of Merit (FOM) begins. To achieve a better result, we only change the refractive index of the middle ring. We change the refractive index of the rim with a step of 0.01 nm, from 1 to 1.12 nm, which leads to a change in the spectra and resonance wavelength. The transmission spectrum resulting from the refractive index change in the sensor structure is shown in Fig.4.

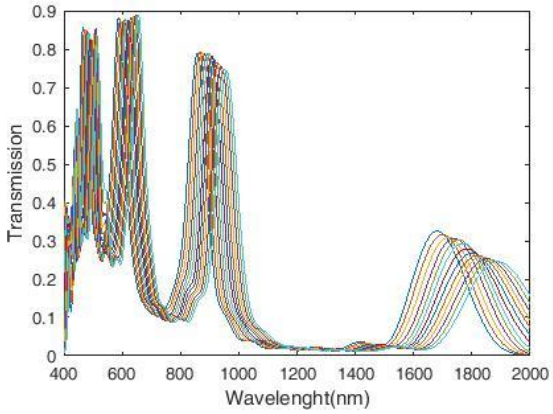

Figure 4: Plasmonic refractive index sensor transmission spectra

The wavelength transmission spectrum has four peaks. The first and most important factor to evaluate the performance of the refractive index sensor is sensitivity. Sensitivity is described as the change in resonant wavelength when the dielectric changes unit. The sensor sensitivity equation is expressed as follows:

$$S = \Delta\lambda / \Delta n \quad (\text{nm/RIU}) \qquad (8)$$

Here, $\Delta\lambda$ is the change in resonance wavelength and Δn is the change in refractive index. According to Fig.5, the maximum sensitivity for the refractive index is n = 1.12 (in mode 4), which is equal to 2832 nm / RIU.

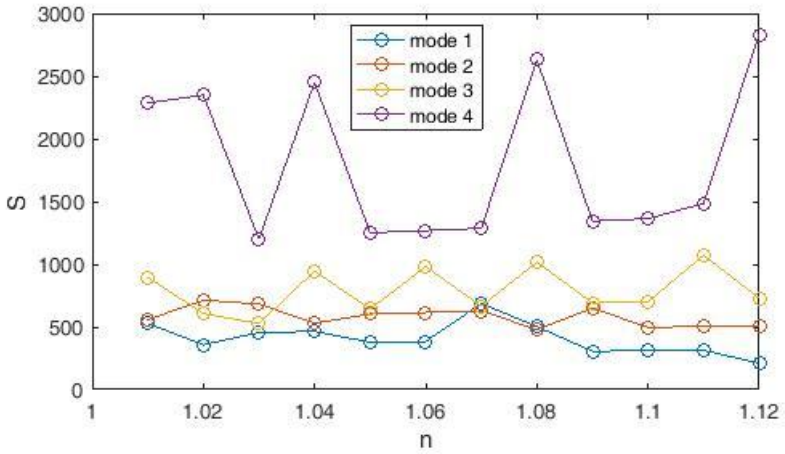

Figure 5: Sensitivity for the structure with the proposed parameters.

The second factor to evaluate the sensor performance is the Figure of Merit (FOM) and its equation is as follows:

$$FOM = S / FWHM \qquad (9)$$

According to Figure 6, the maximum Figure of Merit (FOM) for the refractive index is n = 1.07 (in mode 1), which is equal to 15.1.

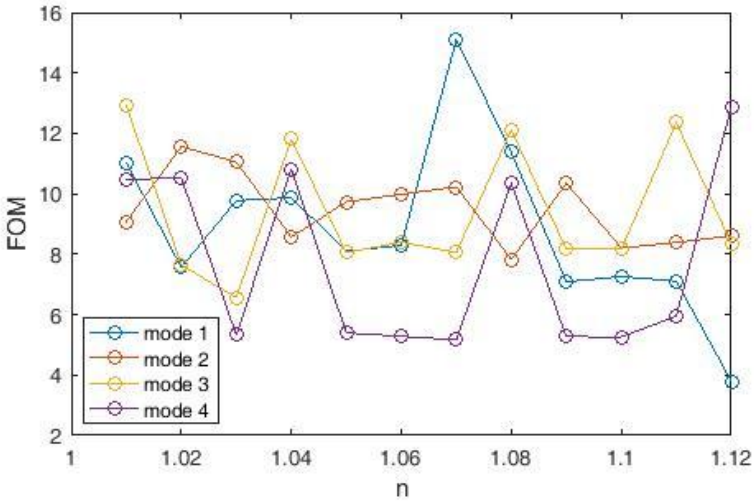

Figure 6: Plasmonic sensor Figure of Merit (FOM) with the proposed parameters.

4. Increase the Number of Resonators

In this step, we increase the number of middle rings to 3 (Fig.7). The dimensions and coordinates of the cavities have not changed and the three rings have an inner radius of r = 152 nm and an outer radius of R = 192 nm. We change the refractive index of the three rings with a step of 0.01 nm, from 1 to 1.12 nm and we obtain the transfer spectrum resulting from the change of the refractive index in the structure (Fig.8). The wavelength transmission spectrum has three peaks.

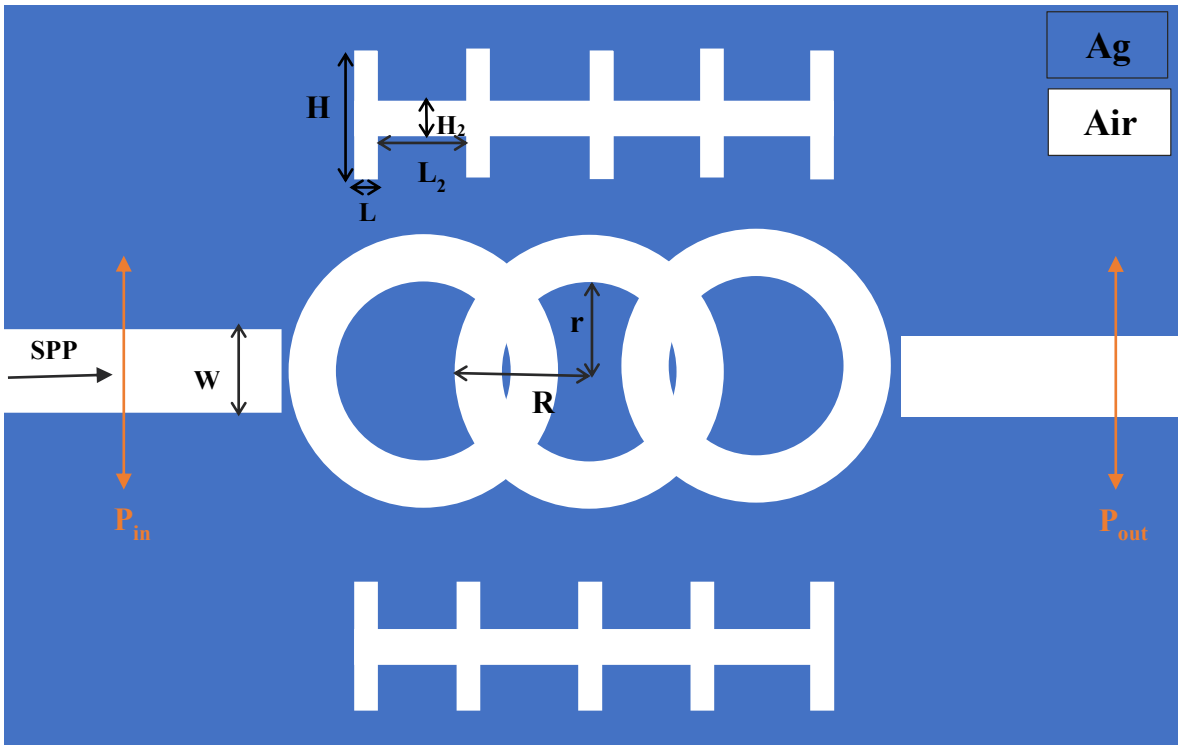

Figure 7: Two-dimensional image of the proposed plasmonic sensor.

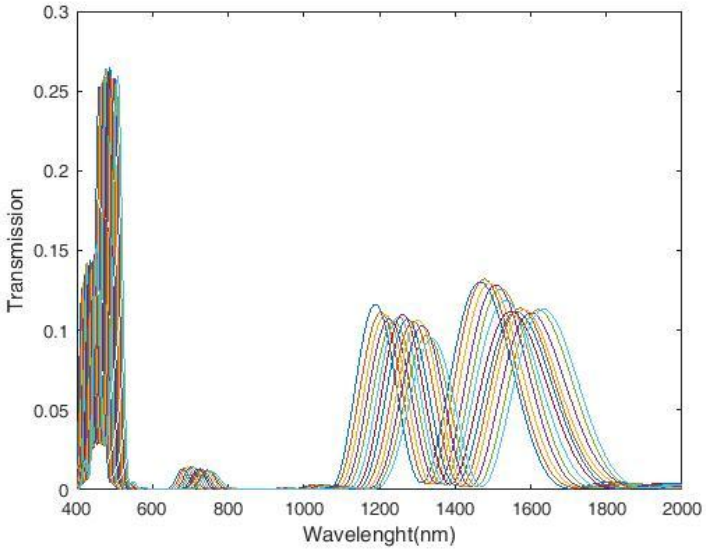

Figure 8: Plasmonic refractive index sensor transmission spectra.

We examine the Field distribution | Hz | at three peaks of the resonant wavelength (Figure 9). The field distribution | Hz | indicates in which part of the sensor structure the electromagnetic field is concentrated. We conclude that at wavelength of 585 nm, the maximum radiation is in the left ring. At wavelength of 1336 nm, the maximum radiation is in all three rings At wavelength of 1633 nm, the maximum radiation is in the left and right rings. Thus, the fano resonance is the result of the interaction between the narrow resonance due to the three rings and the wide resonance due to the MIM.

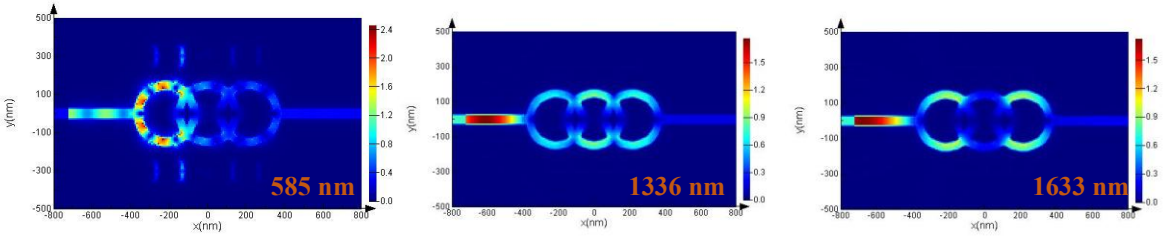

Figure 9: shows the field distribution | Hz | in structure at resonant wavelengths λ = 465.7 nm, λ = 585 nm, λ = 1336 nm and λ = 1633 nm.

Using Equation 8, we obtain the graph of the proposed sensor sensitivity (Fig.10). According to the figure, the maximum sensitivity for the refractive index is n = 1.11 (in mode 3), which is equal to 2083 nm / RIU.

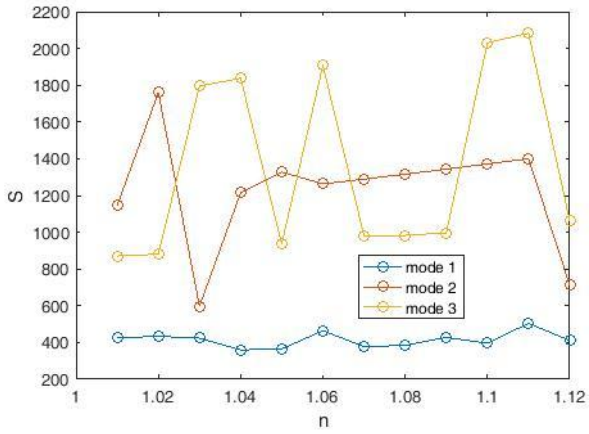

Figure 10: Sensitivity for the structure with the proposed parameters.

Also, using Equation 9, we obtain the diagram for the Figure of Merit (FOM) (Fig.11). According to the figure, the maximum Figure of Merit (FOM) for the refractive index is n = 1.06 (in mode 1), which is equal to. 18.9.

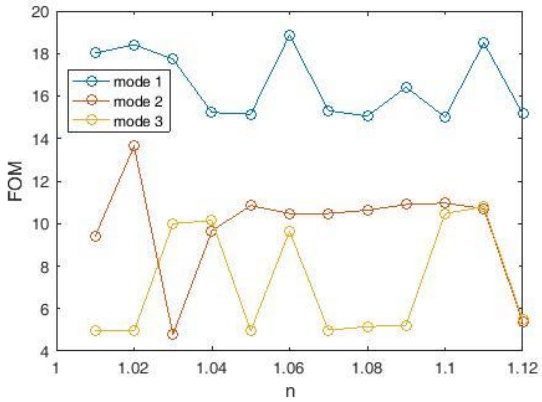

Figure 11: Plasmonic sensor Figure of Merit (FOM) with the proposed parameters.

In these two proposed sensors with new sizes, two Fano resonance points with good sensitivity and Figure of Merit (FOM) values have been produced, which can be used to build a high sensitivity refractive index sensor.

Conclusion

In this paper, a simple structure refractive index sensor including two MIM waveguides, three rings, two cavities and twenty teeth based on surface plasmon is proposed and simulated and investigated by FDTD numerical method with PML adsorption boundary conditions. In the initial configuration, the sensitivity is calculated by changing the refractive index of the structure and the best value is 2832 nm / RIU at the resonant wavelength. Due to the importance of Figure of Merit (FOM) in sensors, the value of this parameter was calculated in the same structure and the best value of 15.1 was obtained. Also, by increasing the number of rings, the sensitivity is calculated and the best value of 2083 nm / RIU is obtained during the resonant wavelength. The Figure of Merit (FOM) value was calculated in the same structure and the best value was 18.9. The most important feature of the structure introduced in this article is high sensitivity and ease of construction. Also, the sensitivities have the same and regular rhythm and increase with the change of the refractive index. This sensor has been considered because it causes a significant change in the propagation characteristics of the wave with a small change in the refractive index. Plasmonic refractive index sensor is a broad topic and because a small change in the refractive index of the causes a large change in the propagation properties of the wave, it has become very popular in the field of chemical and biological measurements.

References

1. Barnes, W. L., Dereux, A., & Ebbesen, T. W. (2003). Surface plasmon subwavelength optics. nature, 424(6950), 824-830.
2. Hassan, M. F., Hasan, M. M., Ahmed, M. I., & Sagor, R. H. (2020, July). Numerical investigation of a plasmonic refractive index sensor based on rectangular MIM topology. In 2020 International Seminar on Intelligent Technology and Its Applications (ISITIA) (pp. 77-82). IEEE.
3. Fang, Y., & Sun, M. (2015). Nanoplasmonic waveguides: towards applications in integrated nanophotonic circuits. Light: Science & Applications, 4(6), e294-e294.
4. Wu, W., Yang, J., Zhang, J., Huang, J., Chen, D., & Wang, H. (2016). Ultra-high resolution filter and optical field modulator based on a surface plasmon polariton. Optics letters, 41(10), 2310-2313.
5. Lai, W., Wen, K., Lin, J., Guo, Z., Hu, Q., & Fang, Y. (2018). Plasmonic filter and sensor based on a subwavelength end-coupled hexagonal resonator. Applied Optics, 57(22), 6369-6374.
6. Wu, D., Liu, C., Liu, Y., Yu, L., Yu, Z., Chen, L., ... & Ye, H. (2017). Numerical study of an ultra-broadband near-perfect solar absorber in the visible and near-infrared region. Optics letters, 42(3), 450-453.
7. Yu, Y., Si, J., Ning, Y., Sun, M., & Deng, X. (2017). Plasmonic wavelength splitter based on a metal–insulator–metal waveguide with a graded grating coupler. Optics letters, 42(2), 187-190.
8. Chen, L., Liu, Y., Yu, Z., Wu, D., Ma, R., Zhang, Y., & Ye, H. (2016). Numerical analysis of a near-infrared plasmonic refractive index sensor with high figure of merit based on a fillet cavity. Optics express, 24(9), 9975-9983.
9. Tsigaridas, G. N. (2017). A study on refractive index sensors based on optical micro-ring resonators. Photonic Sensors, 7, 217-225.
10. Tong, L., Wei, H., Zhang, S., & Xu, H. (2014). Recent advances in plasmonic sensors. Sensors, 14(5), 7959-7973.
11. Shen, Y., Zhou, J., Liu, T., Tao, Y., Jiang, R., Liu, M., ... & Wang, J. (2013). Plasmonic gold mushroom arrays with refractive index sensing figures of merit approaching the theoretical limit. Nature communications, 4(1), 2381.
12. Srivastava, T., Das, R., & Jha, R. (2013). Highly sensitive plasmonic temperature sensor based on photonic crystal surface plasmon waveguide. Plasmonics, 8, 515-521.
13. Maisonneuve, M., Kelly, O. D. A., Blanchard-Dionne, A. P., Patskovsky, S., & Meunier, M. (2011). Phase sensitive sensor

on plasmonic nanograting structures. Optics express, 19(27), 26318-26324.
14. Elsayed, M. Y., Ismail, Y., & Swillam, M. A. (2017). Semiconductor plasmonic gas sensor using on-chip infrared spectroscopy. Applied Physics A, 123(1), 113.
15. Chen, Z., Yu, L., Wang, L., Duan, G., Zhao, Y., & Xiao, J. (2015). Sharp asymmetric line shapes in a plasmonic waveguide system and its application in nanosensor. Journal of Lightwave Technology, 33(15), 3250-3253.
16. Tang, Y., Zhang, Z., Wang, R., Hai, Z., Xue, C., Zhang, W., & Yan, S. (2017). Refractive index sensor based on Fano resonances in metal-insulator-metal waveguides coupled with resonators. Sensors, 17(4), 784.
17. Zhang, Z., Luo, L., Xue, C., Zhang, W., & Yan, S. (2016). Fano resonance based on metal-insulator-metal waveguide-coupled double rectangular cavities for plasmonic nanosensors. Sensors, 16(5), 642.
18. Zafar, R., & Salim, M. (2015). Enhanced figure of merit in Fano resonance-based plasmonic refractive index sensor. IEEE Sensors Journal, 15(11), 6313-6317.
19. Zhao, X., Zhang, Z., & Yan, S. (2017). Tunable Fano resonance in asymmetric MIM waveguide structure. Sensors, 17(7), 1494.
20. Chen, J., Li, Z., Zou, Y., Deng, Z., Xiao, J., & Gong, Q. (2013). Coupled-resonator-induced Fano resonances for plasmonic sensing with ultra-high figure of merits. Plasmonics, 8, 1627-1631.
21. Wang, J., Liu, X., Li, L., He, J., Fan, C., Tian, Y., ... & Liang, E. (2013). Huge electric field enhancement and highly sensitive sensing based on the Fano resonance effect in an asymmetric nanorod pair. Journal of Optics, 15(10), 105003.
22. Bianconi A (2002) Ugo Fano and shape resonances, AIP Conference Proceedings, 19th Int. Conference Roma June 24- 28, 2002.
23. Yang, Q., Liu, X., Guo, F., Bai, H., Zhang, B., Li, X., ... & Zhang, Z. (2020). Multiple Fano resonance in MIM waveguide system with cross-shaped cavity. Optik, 220, 165163.
24. Chen, J., Li, J., Liu, X., Rohimah, S., Tian, H., & Qi, D. (2021). Fano resonance in a MIM waveguide with double symmetric rectangular stubs and its sensing characteristics. Optics communications, 482, 126563.
25. Maier, S. A. (2007). Plasmonics: fundamentals and applications (Vol. 1, p. 245). New York: springer.
26. Yan, S. B., Luo, L., Xue, C. Y., & Zhang, Z. D. (2015). A refractive index sensor based on a metal-insulator-metal waveguide-coupled ring resonator. Sensors, 15(11), 29183-29191.
27. Huang, Y. X., Xie, Y. Y., Zhao, W. L., Che, H. J., Xu, W. H., Li, X., & Li, J. C. (2014, August). A plasmonic refractive index sensor based on a MIM waveguide with a side-coupled nanodisk resonator. In 2014 IEEE 20th International Conference on Embedded and Real-Time Computing Systems and Applications (pp. 1-5). IEEE.
28. Wu, T., Liu, Y., Yu, Z., Ye, H., Peng, Y., Shu, C., ... & He, H. (2015). A nanometeric temperature sensor based on plasmonic waveguide with an ethanol-sealed rectangular cavity. Optics Communications, 339, 1-6.
29. Xiao, G., Xu, Y., Yang, H., Ou, Z., Chen, J., Li, H., ... & Li, J. (2021). High sensitivity plasmonic sensor based on Fano resonance with inverted U-shaped resonator. Sensors, 21(4), 1164.
30. Achi, S. E., Hocini, A., Salah, H. B., & Harhouz, A. (2020). Refractive index sensor MIM based waveguide coupled with a slotted side resonator. Progress In Electromagnetics Research M, 96, 147-156.
31. Barnes, W. L., Dereux, A., & Ebbesen, T. W. (2003). Surface plasmon subwavelength optics. nature, 424(6950), 824-830.
32. Schuller, J. A., Barnard, E. S., Cai, W., Jun, Y. C., White, J. S., & Brongersma, M. L. (2010). Plasmonics for extreme light concentration and manipulation. Nature materials, 9(3), 193-204.
33. Khurgin, J. B. How to face the loss in plasmonics and metamaterials. Nature Nanotechnology 2014, 10(1), 2-6.
34. Fang, Y., Wen, K., Li, Z., Wu, B., Chen, L., Zhou, J., & Zhou, D. (2019). Multiple Fano resonances based on end-coupled semi-ring rectangular resonator. IEEE photonics journal, 11(4), 1-8.
35. Sagor, R. H., Hassan, M. F., Yaseer, A. A., Surid, E., & Ahmed, M. I. (2021). Highly sensitive refractive index sensor optimized for blood group sensing utilizing the Fano resonance. Applied Nanoscience, 11, 521-534.